Comprehensive analysis of major fault-to-failure mechanisms in harmonic drives

machines

MDPI

Article

Comprehensive Analysis of Major Fault-to-Failure Mechanisms in Harmonic Drives

Roberto Guida *, Antonio Carlo Bertolino, Andrea De Martin and Massimo Sorli

Department of Mechanical and Aerospace Engineering, Politecnico di Torino, Corso Duca degli Abruzzi 24, 10129 Torino, Italy; antonio.bertolino@polito.it (A.C.B.); andrea.demartin@polito.it (A.D.M.); massimo.sorli@polito.it (M.S.)

* Correspondence: roberto.guida@polito.it

Abstract: The present paper proposes a detailed Failure Mode, Effects, and Criticality Analysis (FMECA) on harmonic drives, focusing on their integration within the UR5 cobot. While harmonic drives are crucial for precision and efficiency in robotic manipulators, they are also prone to several failure modes that may affect the overall reliability of a system. This work provides a comprehensive analysis intended as a benchmark for advancements in predictive maintenance and condition-based monitoring. The results not only offer insights into improving the operational lifespan of harmonic drives, but also provide guidance for engineers working with similar systems across various robotic platforms. Robotic systems have advanced significantly; however, maintaining their reliability is essential, especially in industrial applications where even minor faults can lead to costly downtimes. This article examines the impact of harmonic drive degradation on industrial robots, with a focus on collaborative robotic arms. Condition-Based Maintenance (CBM) and Prognostics and Health Management (PHM) approaches are discussed, highlighting how digital twins and data-driven models can enhance fault detection. A case study using the UR5 collaborative robot illustrates the importance of fault diagnosis in harmonic drives. The analysis of fault-to-failure mechanisms, including wear, pitting, and crack propagation, shows how early detection strategies, such as vibration analysis and proactive maintenance approaches, can improve system reliability. The findings offer insights into failure mode identification, criticality analysis, and recommendations for improving fault tolerance in robotic systems.

Keywords: harmonic drive; fault-to-failure mechanisms; FMECA; PHM

Citation: Guida, R.; Bertolino, A.C.; De Martin, A.; Sorli, M. Comprehensive Analysis of Major Fault-to-Failure Mechanisms in Harmonic Drives. *Machines* **2024**, *12*, 776. https://doi.org/10.3390/machines12110776

Received: 2 October 2024
Revised: 30 October 2024
Accepted: 4 November 2024
Published: 5 November 2024

1. Introduction

Harmonic drives, also known as strain wave gears, are widely used in various precision motion control systems due to their high torque-to-weight ratio, compact design, and low backlash capabilities [1]. These characteristics make them critical components in applications such as robotics [2], aerospace [3], and industrial automation [4].

In these fields, reliability is paramount, as any component failure can lead to severe operational, financial, and safety consequences. Harmonic drives provide high torque with minimal backlash within a compact structure, supporting precise motion control, stable positioning, and the capacity to withstand variable loads. These qualities are especially valuable in collaborative robots (cobots) that work alongside humans in industrial environments, and their reliability ensures that harmonic drives can handle continuous, repetitive tasks in close proximity to human workers without unexpected malfunctions, which could otherwise compromise safety and productivity. For aerospace applications, the lightweight yet highly reliable design of harmonic drives supports critical actuation mechanisms used in flight control surfaces, satellite deployment systems, and other high-stake applications. Given the extreme conditions and stringent reliability requirements in aerospace, any drive failure could impact mission success and compromise safety, requiring costly repairs or replacements.

However, despite their numerous advantages, harmonic drives are subject to various fault-to-failure mechanisms that can significantly impact performance and reliability. Understanding these mechanisms is essential for improving the longevity and operational efficiency of harmonic drives, especially in high-stake applications where failure can lead to costly downtime or potentially catastrophic system failures.

The harmonic drive consists of three main components: the wave generator (WG), the flexspline (FS), and the crcular spline (CS) (Figure 1). The WG is composed of an elliptical thin-raced ball bearing mounted on the motor shaft. When inserted into the FS, a flexible, cylindrical cup with external teeth, it induces a radial elastic deformation in the FS. This deformation causes the FS to engage with the CS, which is a rigid and internally toothed gear.

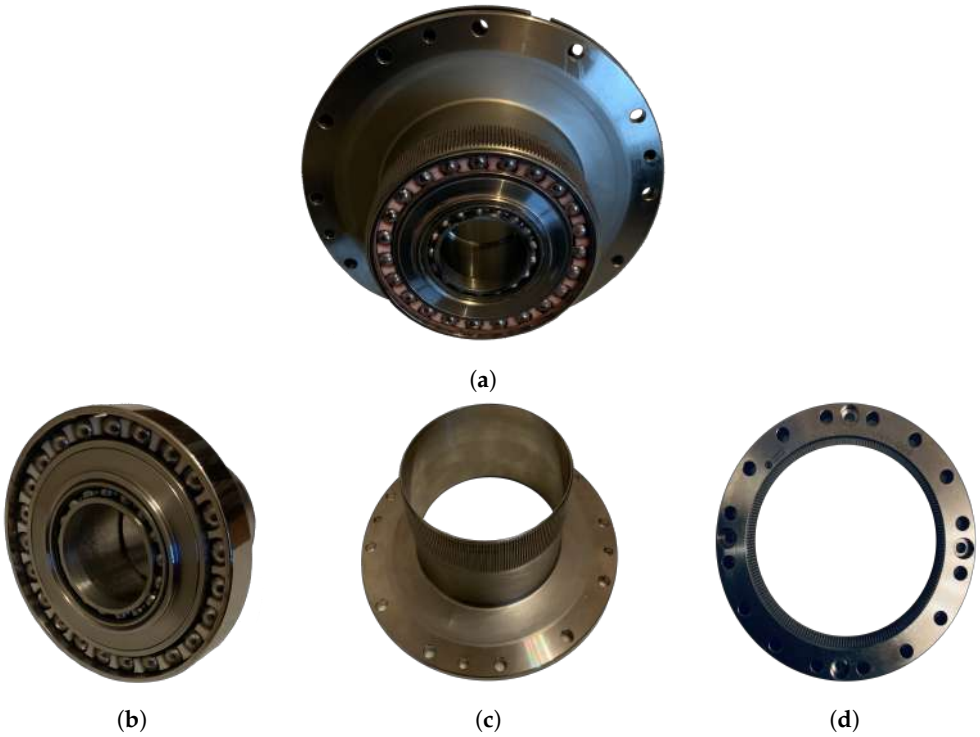

(**a**) (**b**) (**c**) (**d**)

Figure 1. Main components of a (**a**) harmonic drive gear: (**b**) wave generator, (**c**) flexspline, and (**d**) circular spline.

Unlike conventional gears, meshing in a harmonic drive occurs only at two points along the major axis of the elliptical WG. This unique feature allows approximately 20–30% of the teeth to be in continuous contact at any given time [5]. This extensive tooth engagement significantly reduces backlash and enhances the system's positioning accuracy and repeatability, making harmonic drives ideal for precision applications.

This high precision is further enhanced by the use of a double-arc tooth profile [6,7], as shown in Figure 2. This specialized tooth design improves load distribution across the teeth, minimizing wear and maximizing efficiency.

Typically, the FS has two fewer teeth than the CS. This difference in tooth count creates a mechanical advantage, such that with every full rotation of the WG, the output shaft of the harmonic drive moves by only two teeth. This results in a significant reduction ratio (τ), expressed as the ratio between WG angular speed $(\dot{\theta}_{\mathrm{WG}})$ and CS $(\dot{\theta}_{\mathrm{CS}})$ angular speed, which can be calculated using the following equation:

$$\tau = \frac{\dot{\theta}_{\mathrm{WG}}}{\dot{\theta}_{CS}} = \frac{Z_{CS}}{Z_{CS} - Z_{FS}}; \tag{1}$$

where

- Z_{CS} is the number of circular spline teeth;

- Z_{FS} is the number of flexspline teeth.

This reduction ratio is one of the defining characteristics of harmonic drives, allowing for high torque output and precision even in compact systems.

Despite their relatively simple mechanical design, as the research group preliminarily reported in [8], harmonic drives are vulnerable to a variety of potential failure modes [9]: specific types of wear [10], deformation [11], and material fatigue. Factors such as cyclic loading, lubrication failures [12], and thermal stress [13] can contribute to the degradation of key components over time. Additionally, external influences like environmental conditions and improper assembly can accelerate the onset of faults, ultimately leading to failure.

To address these challenges, modern maintenance strategies like predictive maintenance [14] and Condition-Based Maintenance (CBM) have become essential [15]. Predictive maintenance involves forecasting failures based on real-time data, allowing for maintenance actions to be performed only when necessary, which reduces both unplanned downtime and unnecessary maintenance costs. Similarly, Condition-Based Maintenance focuses on continuously monitoring the state of the harmonic drive through various sensors and performance metrics. Maintenance is triggered when the condition of the drive deviates from nominal parameters, ensuring that components are serviced or replaced before a failure occurs.

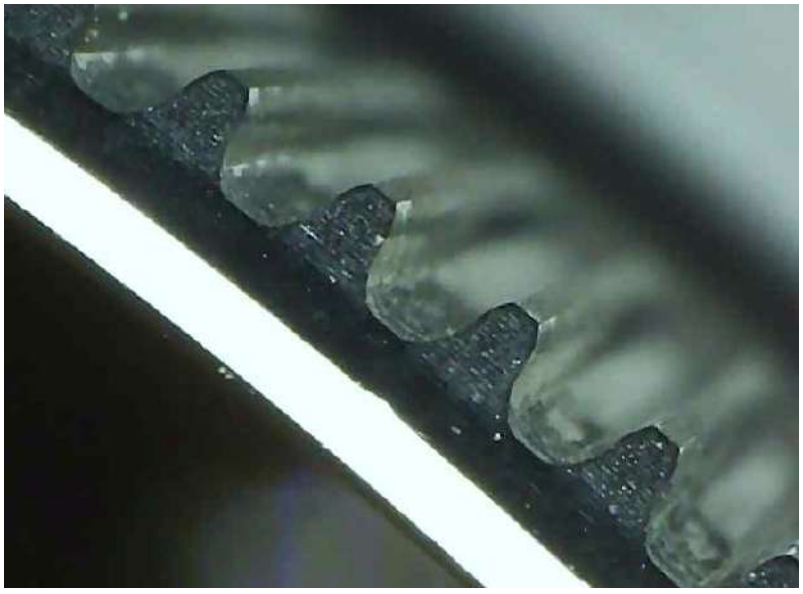

Figure 2. Double-arc profile of the flexspline tooth.

An advanced extension of these approaches is Prognostics and Health Management (PHM) [16], which integrates condition monitoring, diagnostics, and prognostics into a unified framework. PHM systems not only detect current issues but also predict future failures and Remaining Useful Life (RUL) by analyzing the evolution of faults within the harmonic drive. By utilizing a combination of real-time data, machine learning models, and historical failure data, PHM helps optimize maintenance scheduling, reduce operational risks, and enhance the overall reliability of critical systems.

PHM enables real-time condition monitoring, which is crucial for applications where unplanned downtime or unexpected drive failure could lead to significant financial loss, production delays, or, in the worst cases, safety hazards. For example, a collaborative robot malfunction in a production line could result in costly delays, while an unexpected failure in an aerospace mission could necessitate extensive repairs or compromise the mission entirely. PHM's predictive capabilities address these risks by detecting early-stage degradation, allowing for scheduled maintenance that aligns with operational needs. This proactive maintenance approach extends the functional life of harmonic drives, reduces maintenance costs, and ensures that systems continue to perform safely and reliably in

high-stake environments. Through predictive maintenance, PHM minimizes the financial and safety impacts of drive failures, making it essential for supporting the reliability requirements of advanced robotic and aerospace applications.

One of the key challenges in implementing data-driven PHM systems is the availability of sufficient high-quality data. In many cases, historical failure data or real-time operational data may be limited, incomplete, or difficult to obtain for harmonic drives, particularly in new or specialized applications. This lack of data creates uncertainty in the development of accurate predictive models and limits the effectiveness of purely data-driven PHM approaches.

To overcome this limitation, a model-based approach can be employed, developing a high-fidelity model capable of simulating both nominal and non-nominal behavior of the harmonic drive. In this approach, a detailed physics-based digital twin of the harmonic drive is created, capturing the key mechanical and operational characteristics that influence its performance under different conditions. By simulating faults in a digital twin, it is possible to generate data on degraded behaviors, which can be used to train data-driven models (DDMs) for feature selection and anomaly detection [17]. This methodology has been validated not only in robotics [18] but also in the aerospace sector [19–21].

By integrating the model-based approach with PHM frameworks, it becomes possible to predict failures and estimate the RUL of harmonic drives with greater accuracy, even in the absence of extensive operational data. This hybrid approach combines the strengths of both data-driven and model-based methods, providing a robust solution for ensuring the long-term accuracy, repeatability, and reliability of harmonic drives in critical applications.

Real-time performance in mechanical fault diagnosis is essential, particularly in scenarios where timely responses can prevent machinery damage, costly downtime, and potential safety hazards. Fault diagnosis systems designed for real-time processing enable immediate detection and responses to anomalies, which are especially critical in high-stake environments such as manufacturing, aerospace, and power generation.

In the paper by Wang et al. [22], an example of the importance of real-time performance is demonstrated through the Metric SpikingFormer (MSF) model used in the Industrial Internet of Things (IIoT) for mechanical fault diagnosis. In this setup, the MSF operates within energy-limited environments, such as remote monitoring of industrial equipment, where high-frequency, real-time fault detection is crucial for preventing costly breakdowns. By using an event-driven spiking mechanism, the MSF model processes only significant events, which reduces the computational load and conserves energy. This efficient real-time processing allows for immediate fault detection, enabling timely maintenance actions that can prevent minor issues from escalating into major failures.

Real-time performance in fault diagnosis is also crucial for industrial systems like ship propulsion, where delayed detection can lead to severe failures, costly downtime, and safety risks. This study addresses this by proposing a lightweight diagnostic network that minimizes computational load while maintaining high accuracy, even under a data imbalance. This approach ensures timely fault detection and classification, supporting real-time monitoring that meets industry safety and efficiency standards [23].

Future research could leverage emerging technologies like federated learning and large language models (LLMs) to address current limitations in fault diagnosis. Federated learning enables collaborative model training across devices while maintaining data privacy, which is ideal for sensitive industrial settings. Meanwhile, LLMs can enhance data interpretation and anomaly detection, potentially streamlining fault diagnosis. These advancements offer promising pathways to improve adaptability, accuracy, and efficiency in real-time industrial applications.

To support the development and application of these techniques, this paper aims to provide a comprehensive analysis of the major fault-to-failure mechanisms in harmonic drives. By examining both intrinsic factors, such as material fatigue and internal component wear, and extrinsic factors, such as environmental conditions and operational stresses, it offers an in-depth understanding of how these mechanisms evolve and ultimately lead to

failure. The insights gained from this analysis will contribute not only to the development of more effective predictive maintenance strategies but also to the design and optimization of more robust and resilient harmonic drives for future engineering applications.

Building upon previous work, such as the analysis in [8], this study delves deeper into the fault-to-failure mechanisms. Alongside a more detailed examination, this paper introduces a preliminary model that captures the progression of these mechanisms. By incorporating data from faulted components, the model enhances the accuracy of failure predictions and supports more effective maintenance strategies, ultimately improving system reliability in critical applications.

In addition to theoretical modeling, an extensive analysis of faulted components was conducted to investigate the physical manifestations of failure within harmonic drives. Key components such as the flexspline, wave generator, and circular spline were carefully examined post-failure to identify wear patterns, material deformations, and other failure indicators. This component-level analysis has provided critical insights into how operational stresses contribute to specific failure modes, thus offering a practical dimension to the theoretical findings.

Unlike studies that concentrate on isolated fault mechanisms or single failure types, this research adopts a holistic approach by examining multiple interconnected failure modes, such as wear, pitting, and cracking, within a unified framework. This comprehensive perspective allows for a more thorough understanding of how these faults interact and influence one another, ultimately affecting the reliability and performance of harmonic drives in industrial applications. By situating each fault type within its root causes, this study offers a structured pathway for engineers and researchers to anticipate fault progression, thereby serving as a foundational reference for fault diagnostics, early detection, and predictive maintenance strategies.

The outcomes of this research are designed to complement and enhance advanced fault diagnosis techniques. For example, data-driven models like the Neural-transformer, known for its lightweight architecture and efficiency in mechanical fault diagnosis [24], and the Uncertainty Perception Metric Network, effective in diagnosing machinery faults under limited, noisy data conditions [25], can benefit from this study's structured insights into fault progression. By integrating the systematic understanding of fault mechanisms provided here, these and similar methodologies can improve both the accuracy and reliability of their diagnostics, enabling more precise predictions even in complex, noise-prone environments.

2. Harmonic Drive in Cobot Applications

In robotics, harmonic drives are often employed in joints that require fine movements, such as in articulated robotic arms, humanoid robots, and collaborative robots (cobots). Their compact nature allows them to be integrated into smaller form factors without sacrificing performance, a key factor for robots operating in constrained or delicate environments. Additionally, their high torque transmission capability allows robots to manipulate heavier loads while maintaining smooth and accurate motion.

Robots were initially developed to automate repetitive and straightforward tasks, with their primary application being in assembly lines where the outcome of each task is linked to the others [26]. Consequently, a significant fault in a single robot can disrupt the entire production process, resulting in quality degradation, unexpected downtimes, and financial losses.

In recent years, the advent of collaborative robotics has opened the door for small and medium-sized enterprises to adopt industrial automation [27]. Collaborative robots, or cobots, operate in shared environments with human operators, necessitating compliance with the stringent safety standards. Typically, cobots are governed by reactive control algorithms that halt motion when a deviation from the programmed path occurs. However, as noted in [28], these reactive measures may only activate after the operator's safety has already been compromised. Proactive safety can be achieved with collision avoidance

algorithms [29], though these may prove inadequate when the robot is operating under degraded conditions.

Cobots are deemed safe as long as they function under nominal conditions, but this safety cannot be guaranteed in the event of a fault. In this context, Prognostics and Health Management (PHM) techniques represent a breakthrough by significantly enhancing robot availability and ensuring operator safety [30]. Early fault detection allows for tracking degradation and scheduling maintenance before dangerous behavior manifests. PHM approaches often rely on DDMs to extract health indicators (HIs) from the manipulator. However, industrial robots have a mean time between failures (MTBF) that is often measured in tens of thousands of hours [31], resulting in insufficient fault data [32], hampering the performance of DDMs.

Robotic malfunctions can stem from various sources, including damage to the control unit, user interface, or (more frequently) to the joints [33]. Such failures can cause the robot to operate in degraded conditions or even cease functioning altogether. While industrial robots employ several technologies and configurations depending on their intended tasks, most robotic joints consist of five key components: electronics, sensors, motors, reducers, and bearings [34]. Failures in the first three components are often detected by built-in control logic. However, mechanical failures, such as bearing wear, may go unnoticed as control algorithms compensate by increasing motor current, thus masking the issue while allowing the robot to operate in degraded conditions—posing a potential safety hazard.

While this analysis centers on the UR5 (Figure 3), the findings are applicable to harmonic drives in a broad range of mechatronic systems. A robot typically consists of multiple interdependent subsystems, and malfunctions can arise from single failures or a combination of events. As illustrated in the Fault Tree Analysis (FTA) diagram [35,36] in Figure 4, only the branch associated with the reducer is explored, while other branches, represented by diamonds, remain undeveloped for the sake of this analysis. In the proposed FTA, only root causes are reported, while faults such as wear and cracks are omitted, as they are directly linked to or caused by the identified root causes. This approach focuses on the primary factors, simplifying the analysis by excluding intermediate failure mechanisms.

Figure 3. UR5 collaborative robot.

The FTA methodology [37] follows a top-down, deductive approach, visualizing the relationship between the top-level event (TLE) and underlying failure modes through a hi-

erarchical structure of logic gates. Intermediate events are represented by rectangles, while basic events are denoted by circles. The objective of this analysis is to identify the minimal cut sets, i.e., the combinations of component faults or failures, that can lead to a significant degradation of the robot's performance. When a branch of the fault tree is composed of relatively few events or elements with high failure rates, the system's reliability becomes highly compromised. A comprehensive review of FTA, its methodology, and practical applications is provided in [38]. This method is particularly useful for understanding how failures propagate through a system and for pinpointing critical vulnerabilities.

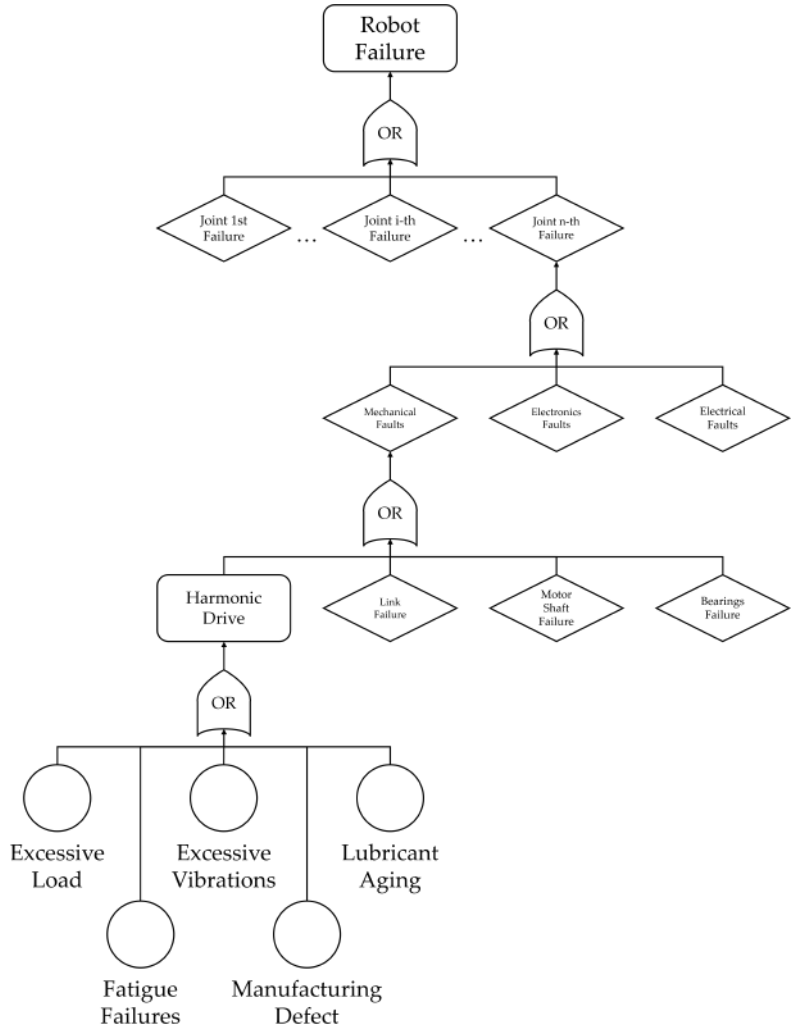

Figure 4. Robot arm fault tree analysis.

In the present analysis, external factors such as collisions, operator errors, and accidental damages are not considered critical for the robot's long-term functioning. These factors can typically be mitigated through correct installation and operation practices. Additionally, empirical data suggest that component failures, such as link breakage or control unit malfunction, are relatively rare occurrences and therefore do not represent the most significant risks to the robot's performance.

In contrast, joint failures, especially those related to complex and heavily loaded components, like the harmonic drive, are far more likely. Each joint plays a vital role in the robot's motion, and a malfunction in even one can compromise the entire operation. As a result, these events are connected via OR gates in the fault tree, signifying that a fault in any single joint could lead to a system-level failure. The same logic applies when examining

the subcomponents within each joint and their respective failure modes, with a specific emphasis on harmonic drive failures.

3. Analysis of Faults Affecting the Harmonic Drive Performances

To study fault nucleation and the progression of failures within the harmonic drive, it is essential to gain a deep understanding of which components are most susceptible to failure and the underlying reasons for their vulnerability. This knowledge will facilitate the development of more accurate prognostic models and allow for the early detection of faults, which is critical in applications where failure could result in significant operational downtime or safety risks.

In this section, a phenomenological analysis aimed at exploring the general mechanisms of degradation and propagation within the studied system is provided. The formulations and equations presented came from the existing literature and are included here as illustrative examples of how propagation phenomena can be modeled. Rather than developing a novel mathematical framework, this paper emphasizes the understanding of underlying physical behaviors and trends associated with degradation.

3.1. Ratcheting and Buckling

A potential failure mode of harmonic drives occurs when excessive torque is applied, which can be due to external factors such as an accidental impact, improper handling, or incorrect transportation. In the case of a rotating gear, an overload condition can cause the CS and FS teeth to fail to engage properly. This misalignment leads to a phenomenon known as ratcheting, where the FS and CS experience eccentric motion [39]. It results in increased eccentricity between the two components, leading to excessive vibrations, accelerated wear, and potentially damaging other parts of the drive.

In the context of robotics, this failure mode can occur in scenarios involving sudden impacts, such as when the robot collides with a human operator or an external object. This is particularly concerning in collaborative robotics applications, where the proximity between robots and human workers increases the likelihood of such collisions. In these cases, collision avoidance algorithms play a crucial role, not only in ensuring the safety of the operator but also in protecting the mechanical integrity of the manipulator [40]. These algorithms are designed to detect and respond to external forces, preventing the application of excessive loads that could compromise the gearbox.

On the other hand, when an excessive load is applied while the input shaft is stationary, the FS tends to experience buckling [41]. Buckling occurs when the FS, due to its flexible nature, deforms under high stress, particularly in the presence of axial loads. While the gearbox may not cease to function immediately, the deformation results in a loss of flexibility. Over time, this leads to a failure in the diaphragm of the FS, which can shear off from the FS cup. This failure mode, described in [42], is especially dangerous because it can compromise the entire drive mechanism if not addressed promptly.

Preventative measures against these overload scenarios are crucial in maintaining the longevity and functionality of harmonic drives in industrial robots. For instance, careful load monitoring and impact detection systems can be implemented to ensure that loads remain within the allowable torque limits [43]. In addition, proper handling and transportation procedures should be followed to avoid any unnecessary stresses on the drive during non-operational phases. In collaborative robotics, where human–robot interactions are frequent, ensuring that force and torque sensors are calibrated to detect abnormal loading conditions can significantly reduce the risk of these failure modes.

Considering that ratcheting refers to progressive, cyclic plastic deformation under stress, it is possible to use Chaboche's plasticity model [44,45] to capture the cyclic hardening/softening behavior of the material and predict the progressive accumulation of plastic strain [46] in the harmonic drive components under cyclic loading.

Ratcheting primarily reduces the stiffness of flexible components within the harmonic drive, particularly affecting the flexspline. This phenomenon leads to a progressive alter-

ation of the mechanical properties, reducing the overall stiffness and compromising the precise deformation capabilities of the flexspline. The progressive accumulation of plastic strain during cyclic loading is modeled by coupling kinematic hardening (via back stress evolution) with the viscoplastic strain rate equation.

The flexspline initially behaves like a flexible elastic shell, with its stiffness (Equation (2)) being determined by its material properties, Young's modulus (E) and Poisson ratio (ν), and geometric properties, like thickness and radius. Under moderate loads, the flexspline returns to its original shape after elastic deformation (ε_e), governed by Hooke's law [47].

$$K_{FS} = f(E, \nu); \tag{2}$$

When the flexspline undergoes cyclic loading, plastic strain (ε_p) accumulates over time due to repeated deformation. As this plastic deformation occurs, the material's stiffness changes, since a portion of the deformation becomes irreversible. This could be captured by the plastic strain in the simplified Chaboche model. Chaboche's viscoplasticity model describes the time-dependent plastic behavior of materials by decomposing total strain into elastic, plastic, and viscous components. It incorporates a flow rule that defines the onset of plastic deformation based on stress and time, using internal variables to capture history-dependent effects and hardening behavior. The model accounts for rate-dependent phenomena, like creep and relaxation, making it widely applicable in engineering for materials subjected to cyclic or long-term loads [44].

The plastic strain rate (ε_p) is obtained as the product between the plastic multiplier (λ) and the derivative of the yield function (f_y) respect to the stress (σ), as shown in Equation (3).

$$\dot{\varepsilon}_p = \lambda \cdot \frac{\delta f_y}{\delta \sigma}; \tag{3}$$

The plastic multiplier controls the inelastic strain rate and reflects the rate of plastic flow. It is influenced by the yield function, and its evolution depends on the material parameters and stress state. The yield function defines the boundary between elastic and plastic regions in the stress space. When the stress state reaches the yield surface, plastic deformation begins. For the Chaboche model, the yield function incorporates kinematic hardening (back stress) and isotropic hardening components.

Permanent plastic deformation leads to a softening of the material in some cases (due to microstructural changes), or hardening in others (if the material becomes more resistant to further deformation). These effects directly reduce the effective stiffness of the flexspline. In ratcheting, plastic strain accumulates in one direction, leading to progressive deformation under cyclic loads. With each cycle being subjected to kinematic hardening, captured by back stress (α), this allows the material to accumulate plastic strain while shifting the yield surface.

$$\dot{\alpha} = C\dot{\varepsilon}_p - \gamma \cdot \alpha \cdot \lambda; \tag{4}$$

where C and γ are material constants for the kinematic hardening evolution.

The evolution of α helps determine when and where plastic deformation occurs during cyclic loading. In this way, it is possible to treat the material as not purely isotropic, capturing the Bauschinger effect, where the material yields at different stress levels depending on the direction of loading [48]. Back stress represents the kinematic hardening component and is used to model the Bauschinger effect, which describes changes in material resistance upon load reversal. It evolves with the plastic strain and accounts for the directional shift of the yield surface in stress space during cyclic loading.

The Chaboche model assumes that the yield surface moves as plastic deformation accumulates, which is described by α. The stress at which yielding starts is no longer centered at the origin of stress space; it shifts as the material deforms plastically:

$$f_y = |\sigma - \alpha| - \sigma_y;$$
$$\frac{\delta f_y}{\delta \sigma} = \frac{\sigma - \alpha}{|\sigma - \alpha|}; \quad (5)$$

where σ_y is the yielding stress.

When α increases, the yield surface shifts, making it harder for the material to continue deforming plastically unless the applied stress increases further. When α decreases (e.g., in the reverse loading direction), the yield surface shifts back, allowing plastic deformation to occur more easily in that direction. This shifting influences the rate of plastic strain by controlling the magnitude of the effective stress.

Furthermore, this shift ensures that the material can continue to deform plastically in different directions, depending on how back stress evolves. It prevents the material from yielding at the same stress level in every cycle, allowing for a more accurate prediction of cyclic behavior.

As the plastic strain increases, the elastic response of the flexspline diminishes over time, meaning that the effective stiffness decreases. As a larger portion of the total strain becomes plastic and does not contribute to elastic recovery and in severe cases, this ratcheting can result in local buckling or fracture, significantly reducing stiffness. This is particularly important in harmonic drives, where the flexspline undergoes repeated deformation.

It is possible to evaluate a new Young's modulus linked to plastic deformation in order to evaluate a new value of the FS stiffness.

$$E' = E - \kappa \cdot \varepsilon_p; \quad (6)$$

where κ is a material-dependent constant that relates plastic strain to a stiffness reduction.

By evaluating the stress caused by ratcheting and solving the system of equations defined by the Chaboche model, it is possible to derive an updated Young's modulus that accounts for material degradation or plasticity effects. This updated modulus reflects the altered mechanical properties due to inelastic strain accumulation. Using this revised modulus, the new, reduced stiffness of the flexspline can be accurately calculated, providing a more realistic representation of its structural response under continued loading conditions.

3.2. Lubrication

In harmonic drive systems, effective lubrication is crucial for maintaining optimal performance and longevity [12]. There are three critical areas for lubrication within the system:

- The FS-CS meshing teeth interface;
- The WG bearing;
- The WG-FS interface.

Accelerated Life Tests (ALTs) conducted in [49] have shown that wear between the WG's outer face and the FS's inner surface plays a significant role in the overall efficiency of the harmonic drive, although it does not directly affect the transmission accuracy. Roberts et al. [50] suggest that to assess the lubrication condition at the WG-FS interface, one should evaluate the axial load (F_a) acting on the WG and the output torque (Q) of the gear. The axial load can be expressed as

$$F_a = \frac{2 \cdot Q}{D \cdot \mu \cdot \tan\theta}; \quad (7)$$

where

- D is the gearbox size factor, provided by the manufacturer;
- θ is the pressure angle, typically around 20°;
- μ is the friction coefficient at the WG-FS interface.

The axial load applied to the wave generator is represented by the force transmitted through the elliptical bearing, which in turn induces deformation in the flexspline. This

transmitted force is crucial in generating the desired shape change in the flexspline, enabling effective engagement with the circular spline in harmonic drive mechanisms. However, if the flexspline is too rigid, the flexspline restoring force is amplified, leading to increased resistance to the intended deformation.

However, measuring this axial load directly is feasible only when the gearbox is mounted on a specialized test bench equipped with appropriate sensors. In practical industrial settings, such testing may not always be viable. An alternative method, which does not require dismounting the harmonic drive from the robot arm, involves dynamic parameter identification of the manipulator [51]. This approach estimates both Coulomb and viscous friction coefficients for each joint. However, it is important to note that friction is influenced by numerous factors beyond the state of lubrication alone, which limits the effectiveness of this method for accurately diagnosing lubrication conditions.

The role of axial load on the WG is particularly important in robotic applications where joint velocities follow a trapezoidal motion profile, characterized by periods of acceleration, constant speed, and deceleration. The axial force acting on the WG varies depending on whether the harmonic drive is functioning as a speed reducer or as a brake. Continuous accelerations and decelerations cause the axial load to fluctuate, which, in turn, leads to periodic protrusion of the FS teeth from the CS [52]. These sliding movements also influence the coning angle, a key factor in maintaining proper lubrication within the gearbox [53].

Moreover, the torque experienced by the joints in an industrial manipulator is subject to constant fluctuations due to the cyclical nature of robotic motion. These torque variations result in repetitive changes in the magnitude of the axial force, which can lead to fretting fatigue, a form of wear caused by the repeated oscillatory contact between the teeth of the FS and CS.

Fretting fatigue is a serious concern, as it can compromise the integrity of the system and reduce the harmonic drive's operational life. Proper monitoring and maintenance of lubrication in these critical areas are essential to mitigate the risks of wear and failure. This makes the selection of appropriate lubricants and regular inspection of lubrication conditions crucial in high-duty applications, especially those involving continuous motion and load variations, as seen in robotic systems.

The causes and effects of poor lubrication conditions could be obtained by means of a thermal aging model [54]. Lubricants in harmonic drives degrade over time due to exposure to high temperatures and mechanical stresses. A thermal aging model, typically based on the Arrhenius equation, can predict the rate of degradation as a function of operating temperature and time [55,56].

Furthermore, a contaminant-based degradation model can simulate the effects of particle contamination (metallic debris) in the lubricant, which accelerates wear in contact surfaces.

The total degradation rate could be obtained combining thermal and contamination effects:

$$k_{\text{lub}} = k_{\text{T}} + k_{\text{C}} = A \cdot e^{-\frac{E_{\text{a}}}{R \cdot T}} + B \cdot C; \tag{8}$$

where

- A is the pre-exponential factor (frequency factor);
- E_{a} is the activation energy (J/mol);
- R is the universal gas constant $(8.314\,\text{J/mol} \cdot \text{K})$;
- T is the absolute temperature (K);
- B is the contamination degradation constant (based on contaminant type and amount);
- C is the contamination level (dimensionless, normalized between 0 and 1).

The pre-exponential factor is a constant that reflects the inherent tendency of the lubricant to degrade over time, irrespective of temperature. It represents the frequency of molecular collisions that could potentially lead to degradation. It is specific to the material properties of the lubricant and is influenced by molecular composition and stability.

It essentially scales the degradation rate, setting the baseline before other factors (like temperature and contamination) come into play.

The activation energy is the minimum energy required for the degradation process to continue. It is specific to the chemical characteristics of the lubricant. Higher values indicate that the lubricant is more resistant to thermal degradation, as it needs more energy to start breaking down. This factor makes the lubricant less sensitive to temperature increases. Lower activation energy, on the other hand, makes the lubricant more prone to rapid degradation under elevated temperatures.

The contamination degradation constant is a coefficient that quantifies the impact of contaminants on the degradation process. It represents the material-specific response of the lubricant to the presence of foreign particles, typically metallic debris, which can increase wear. This constant is often determined experimentally and is influenced by both the type and concentration of contaminants.

The contamination level is a dimensionless parameter that represents the concentration of contaminants in the lubricant. This could include particles from metallic debris, dust, or other impurities. A higher value indicates greater contamination, which results in more abrasive interactions within the lubricant, leading to increased wear and degradation. The parameters can vary over time, especially in environments with poor sealing or where external contaminants are introduced, and it can be monitored through lubricant condition monitoring systems.

3.3. Vibrations

According to [5], the primary source of vibrations in harmonic drives arises from the continuous deformation of the flexspline. This deformation can be exacerbated by various factors, including mounting errors, geometric tolerances, and manufacturing defects, all of which can significantly affect reducer performance. It is essential to recognize that these vibrations not only affect the immediate operation of the harmonic drive but can also lead to long-term damage if not properly managed.

A critical parameter in this context is the resonance frequency (f_r), which is defined as

$$f_r = \frac{1}{2\pi}\sqrt{\frac{K_t}{J}} \qquad [\text{Hz}]; \tag{9}$$

where K_t represents the gear torsional stiffness and J denotes the load moment of inertia. The resonance speed (ω_r) of the gearbox output shaft can then be derived as

$$\omega_r = 180 \cdot f_r \cdot \tau; \tag{10}$$

It is crucial to either pass through this resonance speed quickly during acceleration and deceleration phases. Otherwise, this can lead to intensified FS wear and encourage crack propagation, ultimately compromising the integrity of the gearbox.

Furthermore, these vibrations can adversely affect the deformation characteristics of the FS, leading to improper engagement with the CS and irregular coupling with the WG. Such misalignments can cause increased backlash and reduced efficiency, further exacerbating wear and tear.

For a comprehensive understanding of the impact of various factors on harmonic drive vibrations, a detailed investigation by [57] explores how parameters such as flexspline length, thickness, unbalanced loads, and eccentricity influence the vibrational characteristics of harmonic drives. Their research highlights the importance of precise design and assembly processes to mitigate these detrimental effects and ensure optimal performance in robotic applications.

The WG misalignment could be simulated by means of a kinematic model, focusing on how even small angular deviations affect the overall torque transmission and drive performance [58].

The misalignment could be modeled through a roto-translation matrix that depends on the WG angular position. The kinematic error due to misalignment is expressed as a radial displacement, calculated based on the eccentricity values and angular deviations between the CS and the WG. These eccentricities and angular deviations are used to define rotation matrices that link the nominal position of the WG to its actual position when misalignment is present. This method allows for the analysis of the planar equivalent profile of the WG, which is compared to its nominal profile to quantify the radial displacement and the kinematic error resulting from misalignment.

3.4. Pitting

Repetitive stresses that exceed the material's fatigue resistance can lead to pitting, a type of surface failure characterized by the formation of small pits or craters on the tooth surface. This phenomenon tends to be concentrated in the tooth regions closest to the front and gear cross-sections of the FS, as previously discussed. As pitting progresses, small particles of material become detached from the tooth surface. These particles mix with the lubricant, degrading its quality and effectiveness.

Since harmonic drives typically use a single grease lubrication system for all components, the contamination of the lubricant by these wear particles has far-reaching effects. The accumulation of debris can accelerate wear not only on the FS teeth but also on the elliptical bearing of the WG and the contact interface between the WG and FS. As the lubricant's quality deteriorates, friction increases across these critical contact areas, accelerating the overall degradation process. This progressive loss of material, as shown in Figure 5, leads to a cascade of failures that can compromise the entire gearbox.

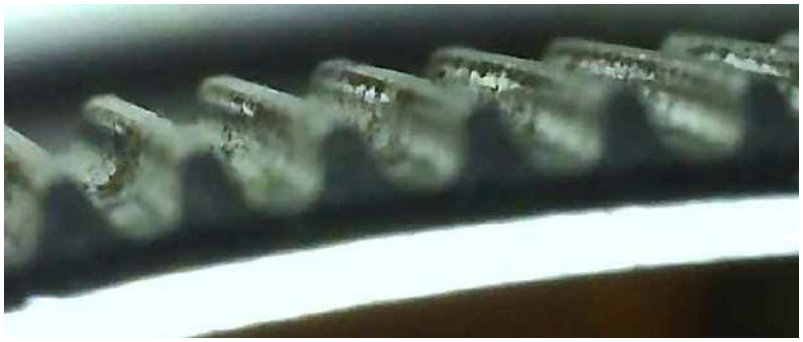

Figure 5. Pitting of the flexspline teeth detected on the shoulder joint of a UR5 collaborative robot.

The presence of pitting accelerates wear, amplifying the potential for backlash and reducing the gearbox's precision over time. In robotic systems, such failures can be detected through the analysis of vibration signals emanating from the robot's joints. Vibration monitoring allows for the early detection of abnormal conditions caused by pitting and wear, enabling maintenance before significant failures occur. Additionally, backlash, which results from the loosening of mechanical contact between components due to material loss, can be observed by comparing the robot's commanded and actual joint positions. Mismatches in these signals often point to a mechanical issue, such as pitting-induced wear.

By detecting these symptoms early through condition monitoring techniques, such as vibration analysis and signal comparison, corrective actions can be taken before pitting leads to more severe gearbox damage. This proactive approach is especially important in systems where harmonic drives are subjected to continuous or cyclical loading, as these conditions are more likely to induce pitting and accelerate the failure process.

A first modeling approach for surface fatigue exploits the Hertzian contact stress model. Since pitting occurs due to surface fatigue from repeated contact stresses, we use a Hertzian contact model to simulate the contact pressure between meshing components (e.g., teeth of the flexspline and circular spline). High contact stresses lead to surface fatigue, initiating pitting [59].

The contact stress for two meshing cylindrical surfaces (as in harmonic drive teeth) can be approximated by

$$\sigma_H = \sqrt{\frac{P \cdot E_{eff}}{\pi \cdot (r_1 + r_2)}}; \quad (11)$$

where

- σ_H is the maximum contact stress (Hertzian stress);
- P is the normal load applied at the contact point;
- E_{eff} is the effective modulus of elasticity depending on the moduli of elasticity of the materials in contact, Poisson's ratios of the materials, and the radii of curvature of the two contacting surfaces;
- r_1 and r_2 are the radii of the two in contact surfaces.

This model allows for the estimation of the stress concentration at contact points, where pitting is most likely to initiate due to fatigue or wear.

A fatigue life model based on S-N curves (stress–life curves) can predict the onset of pitting by estimating the number of cycles before surface fatigue causes failure [60,61].

The relationship between stress and fatigue life is typically expressed as

$$\sigma_H^m \cdot N_f = C_H; \quad (12)$$

where

- σ is the applied stress amplitude (e.g., the Hertzian contact stress);
- N_f is the number of cycles to failure (fatigue life);
- m is the material-specific fatigue exponent, describing how fatigue life decreases with increasing stress;
- C_H is the material constant, determined experimentally from S-N curve data.

3.5. Wave Generator Wear

The wave generator is a key component of the harmonic drive, responsible for creating the strain wave that enables motion transmission. It consists of two primary parts:

- The Elliptical Cam (or Wave Generator Plug): This is the central element of the wave generator. It is typically a rigid, elliptical-shaped component that is inserted into the flexspline. The elliptical shape forces the flexspline to deform, allowing it to engage with the circular spline at specific points. As the wave generator rotates, the deformation of the flexspline continuously changes, creating a wave-like motion.
- The Flexible Bearing: Surrounding the elliptical cam is a flexible bearing, often a thin, high-precision ball bearing. This bearing allows the outer part of the wave generator to rotate smoothly while maintaining the elliptical deformation of the flexspline. The flexible bearing reduces friction and ensures that the wave movement is transferred efficiently to the flexspline without excessive wear.

When the wave generator rotates, it imparts its elliptical shape to the flexspline, causing it to engage with the teeth of the circular spline. This interaction is the core mechanism that allows for the high torque transmission and precise motion control that harmonic drives are known for.

The elliptical ball bearing plays a key role in determining the harmonic drive's operational lifespan. According to [42], the end of life for a harmonic drive is often signaled by the onset of pitting in the inner face of the WG. While the outer face generally fails only under excessive loads, this scenario is particularly problematic, as discussed in the following, due to the ratcheting and buckling effects it induces in the FS. These mechanical stresses can lead to catastrophic failure of the harmonic drive.

One potential method for detecting bearing wear is through the analysis of vibration signals emanating from the robot joint [62]. Vibration analysis is widely used in condition monitoring, where anomalies in the frequency spectrum can reveal early signs of bearing

degradation [63]. Such diagnostic tools could provide valuable insight into the health of the bearing and alert operators to potential issues before they lead to more significant problems.

Another important factor in the degradation of the harmonic drive is wear at the interface between the WG and the FS. This is especially critical in space applications, where improper lubrication in a vacuum environment can lead to metal-on-metal contact between the outer face of the WG and the inner side of the FS cup. As shown in [52], adhesive wear can occur under these conditions, severely affecting the sliding movement between the WG and FS. The severity of the wear is influenced by several factors, including the applied load, operating temperature, and input speed [12]. When the wear becomes significant, it compromises the efficiency and accuracy of the harmonic drive, leading to performance degradation.

The detection of such wear can be achieved by monitoring inconsistencies between the angular positions and velocities of the input and output shafts of the gearbox. A mismatch in these parameters may indicate that the harmonic drive is not functioning as intended, providing an early warning of mechanical degradation.

Additionally, external contaminants can negatively impact the life of the ball bearing. However, this issue has not been considered in the present study, as industrial robots are generally designed to meet specific ingress protection (IP) standards, such as IP54 or IP64. These standards ensure that the robots are protected against dust and limited water ingress, safeguarding internal components. Nevertheless, if robots are operated in harsher environments than they were designed for, and contaminants manage to penetrate the manipulator joint, failure may occur. In such cases, sensors like optical encoders would likely be the first components to cease functioning, as they are highly sensitive to impurities.

The health of the elliptical ball bearing in harmonic drives is crucial for the longevity and reliability of the gearbox. Both wear and improper lubrication can lead to significant performance issues, but with appropriate monitoring techniques such as vibration analysis and angular velocity tracking, these problems can be identified and addressed early. This proactive approach can prevent premature failure and ensure the continued operation of industrial robots in demanding environments.

A stochastic degradation model such as a Wiener process can be used to simulate the gradual wear [64]. The model tracks the increase in wear over time as a random process with drift (representing average wear rate) and noise (random fluctuations in wear) [65].

The Wiener process $W(t)$ is a continuous-time stochastic process defined as

$$X(t) = X_0 + \mu \cdot t + d_{\mathrm{w}} \cdot W(t) \cdot t; \tag{13}$$

where

- $X(t)$ is the state of degradation at time t;
- X_0 is the initial condition (e.g., the initial state of wear);
- μ is the drift coefficient, representing the average rate of wear;
- d_{w} is the diffusion coefficient, representing the variability in the wear process;
- $W(t)$ is a standard Wiener process (Brownian motion), with properties:
  - $W(0) = 0$,
  - $W(t) \sim \mathcal{N}(0, t)$, meaning it follows a normal distribution with mean 0 and variance t.

In this model, it is possible to set a failure threshold such that when $X(t)$ exceeds it, the bearing is considered to have failed and adding periodic maintenance effects modifying the model to include reductions in $X(t)$ due to maintenance activities.

3.6. Meshing Teeth Wear

Industrial manipulators are designed to perform repetitive tasks; as a result, each joint experiences a unique load history and varying levels of wear. For example, in a typical pick-and-place operation, the first three joints of the robot arm are more active, frequently moving within a predefined range of motion. In contrast, the joints of the wrist

tend to remain relatively stationary, as their main function is often to maintain the constant orientation of the Tool Center Point (TCP). This uneven usage can lead to insufficient lubrication of the FS and CS teeth, increasing the likelihood of adhesive wear over time.

As illustrated in Figure 6, the wear on the FS teeth is not uniform but rather exhibits a gradient along its length. The area closer to the input side of the FS shows more severe wear compared to the rear cross-section. This phenomenon is primarily due to the coning angle produced by the insertion of the WG into the FS. When the WG deforms the FS into an elliptical shape, only the input section of the FS undergoes significant deformation, while the rear portion near the FS remains largely circular. This creates an uneven engagement between the FS and CS teeth, leading to an unequal distribution of contact forces along the rotational axis.

In this scenario, the regions near the FS front and the gear cross-sections fully engage with the CS teeth, while the rest of the FS remains partially or entirely disengaged. This uneven meshing results in localized stress concentrations, increasing wear and potentially accelerating failure in the affected areas (Figure 7). Detailed studies on the stresses induced in the FS based on the type of WG used have been proposed in [66,67]. These studies show how design variations can influence wear patterns and overall system longevity.

The presence of wear introduces backlash, a phenomenon where the gear teeth fail to fully engage, resulting in lost motion or play within the system. While modern industrial robots are equipped with encoders to close the position control loop in each joint, backlash is typically compensated for automatically by adjusting motor commands. However, excessive wear and backlash can still degrade the precision of the robot over time. A method for detecting such wear would involve comparing the command signals with feedback signals from the joint's angular positions. Any inconsistencies between these signals—particularly in scenarios where the commanded position does not align with the feedback—may indicate the onset of backlash due to wear.

Figure 6. Effect of the coning angle on flexspline tooth wear.

Furthermore, this form of adhesive wear and backlash can compromise the overall accuracy and repeatability of the manipulator. Continuous monitoring of these parameters is crucial for maintaining the robot's performance, and early detection of wear can prevent further degradation, minimizing downtime and operational inefficiencies.

To properly model these phenomenon, a cumulative damage approach could be followed: the teeth of the flexspline experience cyclical loading, making them susceptible to fatigue. A Palmgren–Miner linear damage rule [68,69] can be applied to model cumulative fatigue damage over time, predicting when the stress cycles will lead to tooth failure.

The reduction in tooth thickness due to abrasive wear between the flexspline and circular spline teeth could be modeled using Archard's law [70,71]:

$$V_{\mathrm{w}} = V_{\mathrm{w}}(t_0) + \int_{t_0}^{t} \frac{K_{\mathrm{w}}}{H_{\mathrm{w}}} \cdot \frac{F_{\mathrm{m}}}{2} \cdot \Delta v_{\mathrm{m}} \, \mathrm{d}t; \tag{14}$$

where V_w is the volume of material removed, K_w is the Archard wear coefficient, H_w is the material hardness, and F_m is the meshing force. The cumulative wear causes a gradual reduction in the effective contact area, degrading the overall torque transmission capability and leading to a loss in motion efficiency.

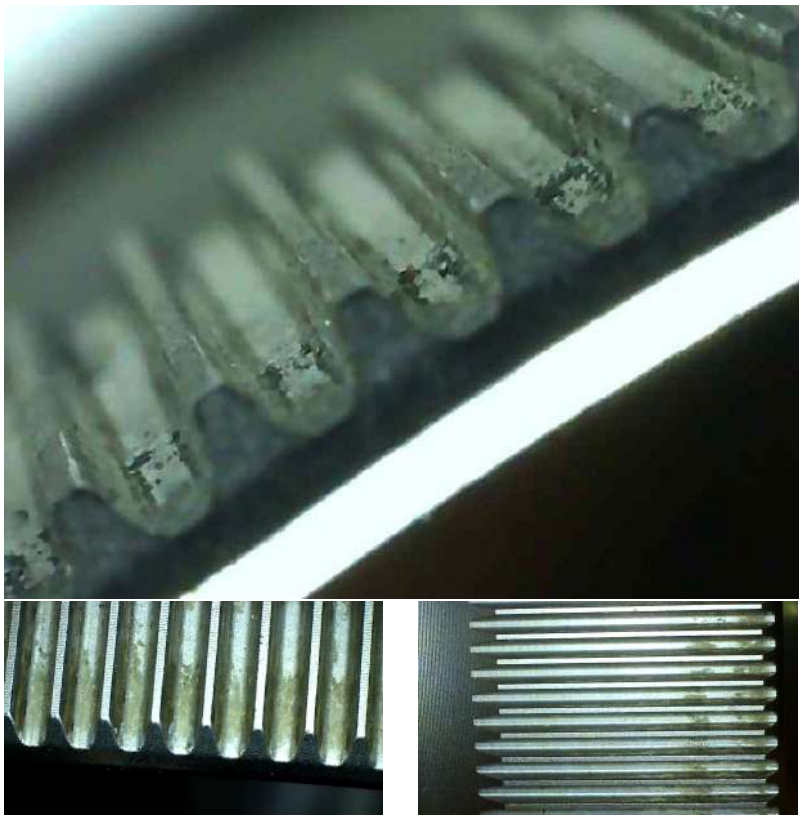

Figure 7. Wear of the flexspline teeth.

4. Faults Affecting the Harmonic Drive Structure Integrity

The most prevalent failure mode observed in harmonic drives is the fatigue fracture of the FS, as highlighted in [72]. This type of failure is particularly concerning because it can compromise the performance and reliability of the entire gearbox system.

Early detection of crack formation is crucial for maintaining operational integrity, and it can be effectively achieved through the analysis of vibration signals emitted by the gearbox. According to [73], specific patterns in these signals can indicate the presence of a crack before it progresses to a catastrophic failure.

The location of the crack significantly influences its propagation behavior and the subsequent impact on the harmonic drive's functionality. Therefore, it is essential to focus on the four most probable regions where crack nucleation may occur: the rim, tooth, rear cross-section, and diaphragm. Each of these areas has distinct stress concentrations and operational demands, making them more susceptible to fatigue.

A representation of the FS, highlighting these critical areas, is provided in Figure 8. This illustration serves as a visual aid for understanding where potential failures might initiate, allowing for targeted inspections and maintenance strategies to be implemented to mitigate the risk of failure.

By focusing on these high-risk regions, it is possible to enhance the longevity and reliability of harmonic drives, ultimately improving the overall performance of robotic systems and other applications that utilize these sophisticated mechanisms.

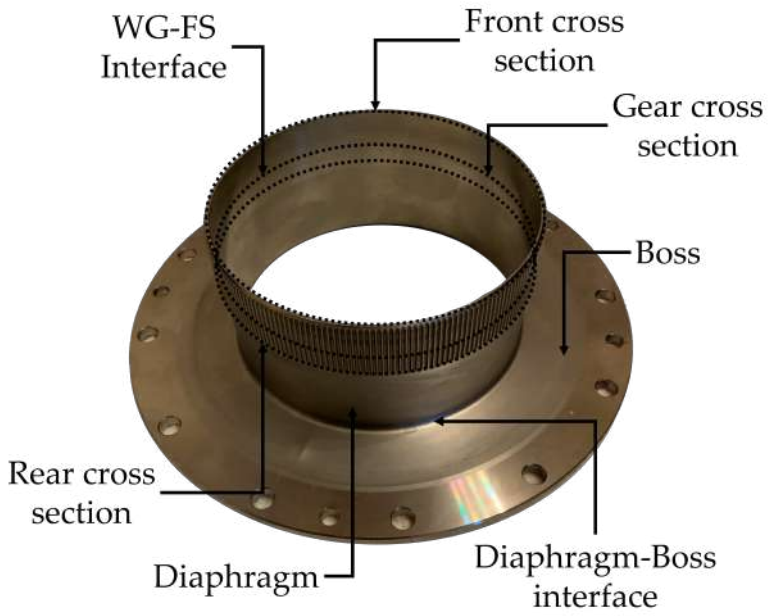

Figure 8. Flexspline of the harmonic drive's critical points for the onset of failures.

A cohesive zone model (CZM) can simulate crack initiation and propagation by defining a traction–separation relationship along the crack path [74]. This is particularly effective for modeling cracks in ductile materials that undergo slow growth before failure. The CZM captures both the elastic and plastic behavior near the crack tip, allowing for an accurate prediction of how the crack grows over time under operational loads.

In the CZM, the crack surface is modeled by cohesive elements, which relate the traction (F_t) (force per unit area) to the separation (δ) (displacement jump across the crack faces).

Before damage initiation, the material behaves elastically.

$$F_t(\delta) = K \cdot \delta; \tag{15}$$

where K is the cohesive stiffness, representing the slope of the traction–separation curve in the elastic regime. Damage begins once the separation reaches a critical value (δ_0), corresponding to the onset of cracks.

$$F_t(\delta_0) = F_{t,max}; \tag{16}$$

where $F_{t,max}$ is the maximum traction force. The separation level refers to the point on the traction–separation curve at which the cohesive elements in the model start to separate under applied stress. It represents the onset of damage in the material, where the traction (or stress) reaches its peak value and micro-cracks begin to form. This point is critical for understanding the point of transition from an intact to a damaged material state within the cohesive zone.

After reaching δ_0, the traction decreases, modeling crack propagation. A linear softening model can be used:

$$F_t = F_{t,max}\left(1 - \frac{\delta - \delta_0}{\delta_f - \delta_0}\right); \tag{17}$$

where δ_f is the final separation at which the material completely fails and the traction reduces to zero. Once the separation reaches δ_f, the material can no longer carry any traction.

$$F_t(\delta_f) = 0; \tag{18}$$

The cohesive stiffness (K) is related to the stiffness of the material in the harmonic drive (e.g., steel or other materials used in the gear). It represents the initial slope of the traction–

separation curve in the cohesive zone model. It describes the resistance of the material to separation at the atomic or molecular level before significant damage occurs. High cohesive stiffness indicates that the material requires a greater force to initiate separation, reflecting a stiffer interface. It is a key parameter for defining the elastic response of the cohesive zone prior to the opening of cracks.

The maximum traction $(F_{t,max})$ represents the maximum stress the material can withstand before damage occurs. The critical separation (δ_0) is the separation at which damage begins (dependent on material toughness). The final separation (δ_f) is the separation at which the material fails completely, linked to the fracture energy of the material. The total energy required to propagate a crack (G_c) can be computed as

$$G_c = \int_0^{\delta_f} F_t(\delta)\, d\delta; \tag{19}$$

Total energy required to propagate the crack is the energy needed to extend the crack through the cohesive zone, often referred to as the fracture energy or work of separation. It is includes the energy required to overcome cohesive forces during crack propagation. This parameter is crucial in determining the toughness of the material, as it quantifies the amount of energy that must be supplied to grow the crack, reflecting the material's resistance to fracture.

This formulation can be implemented to model the crack path in components of a harmonic drive, such as gears or flexsplines, where tooth, rim, or diaphragm cracks are common.

Another common approach for modeling fatigue crack growth is Paris' Law [75], which relates the rate of crack growth to the cyclic stress intensity factor. This model can be used to predict how a crack in the harmonic drive will propagate under repeated loading cycles.

The rate of fatigue crack growth per load cycle $\left(\frac{da}{dN}\right)$ is given by Paris' Law:

$$\frac{da}{dN} = C_P \cdot \Delta K^m \tag{20}$$

where

- a is the crack length.
- N is the number of load cycles.
- C_P and m are material-specific constants.
- ΔK is the range of the stress intensity factor, defined as

$$\Delta K = K_{max} - K_{min}; \tag{21}$$

where K_{max} and K_{min} are the maximum and minimum stress intensity factors during a loading cycle. For a crack in a harmonic drive, which often experiences cyclic loading in the gear teeth or flexspline, the stress intensity factor (K) is related to the applied stress (σ) and the crack length (a):

$$K = \sigma\sqrt{\pi a} \cdot f\left(\frac{a}{w}\right); \tag{22}$$

where

- σ is the applied stress.
- w is the width or relevant dimension of the component.
- $f\left(\frac{a}{w}\right)$ is a geometric correction factor that depends on the crack geometry and the component's geometry.

The material constants C and m are determined experimentally for the specific material used in the harmonic drive (e.g., steel alloys in the gear or flexspline). The stress intensity factor range (ΔK) depends on the loading conditions in the harmonic drive (cyclic stresses due to rotational forces).

4.1. Rim Crack

According to [76], the highest stresses acting on the FS are concentrated at the tooth root surface. When a crack initiates at this location, it can propagate along two distinct paths: either through the tooth (TC) or into the rim (RC) (Figure 9). While both scenarios are undesirable, crack propagation into the rim can lead to catastrophic failure of the harmonic drive.

Figure 9. Crack in the FS rim.

To better understand this phenomenon, one can approximate the FS to a spur gear, allowing the application of relevant studies conducted in [77,78] to this case study. Experimental findings have demonstrated that the backup ratio (b), defined as the ratio of the gear rim thickness (δ) to the tooth height (h), is a critical factor influencing crack propagation behavior. This information is vital for designing a failsafe FS, as its thickness must be optimized to ensure proper engagement with the CS while minimizing the risk of failure.

To mitigate the risk of rim fractures, the use of gears with a backup ratio of $(b \geq 1.3)$ is recommended [79]. A notable example of a successful failsafe design is the harmonic drive employed in the base, shoulder, and elbow joints of the UR5 collaborative robot from universal robots, which boasts a backup ratio of $(b = 2.272)$. This design choice enhances the reliability of the robot by significantly reducing the likelihood of catastrophic failure due to rim cracking.

In contrast, the FS analyzed in [80] exhibits a backup ratio of $(b = 0.576)$. This value falls below the recommended threshold, indicating a substantially higher probability of experiencing catastrophic failure. The differences in backup ratios between various designs underscore the importance of careful engineering considerations in the development of harmonic drives, particularly in applications where reliability and safety are paramount.

4.2. Tooth Crack

Since the FS is subjected to vibrations, especially under heavy loads and high-speed conditions, cracks can also nucleate near the tooth tip, as illustrated in Figure 10. This is largely due to the fact that, although the double-arc tooth profile offers superior performance in terms of positional accuracy, it is associated with higher stress levels compared to an involute tooth profile [81]. The double-arc profile, while beneficial for reducing backlash and improving gear engagement, tends to experience greater localized stress concentrations, particularly under demanding operational conditions.

Unlike the FS, a crack in the CS would typically result in a non-critical failure. This is because the CS generally has a significantly higher backup ratio—often well above

the critical threshold of 1.3, as suggested in [79]. This makes the CS more resilient to catastrophic failure even in the presence of a crack. However, the crack propagation mechanisms in the FS and CS differ considerably due to their structural differences.

In thin-walled gears, [66] have highlighted how the rim thickness influences the load distribution shared by the engaging teeth. Since the force acting on the tooth plays a crucial role in crack initiation and propagation, the difference in backup ratios between the FS and CS must be carefully considered when studying failure modes in harmonic drives. The FS lower backup ratio makes it more susceptible to cracks propagating through the rim, leading to more severe outcomes, while the CS is more robust due to its thicker walls.

Figure 10. Flexspline tooth cracks.

In terms of failure simulation, several studies [82,83] have demonstrated that a tooth crack can be effectively modeled by modifying the teeth meshing stiffness. This approach accurately reflects the reduced load-bearing capacity and altered stress distribution that accompany crack development. Similarly, a rim crack can also be simulated by adjusting the meshing stiffness, as rim cracks tend to have a more pronounced impact on the overall stiffness of the system compared to tooth cracks. The ability to simulate these failure modes is critical for developing early fault detection systems and for designing harmonic drives that can better withstand such stresses.

Tooth cracks typically result from high contact stresses between meshing teeth in the harmonic drive. A Hertzian contact stress model [84] can simulate the stresses at the point of contact, helping to predict the formation of cracks due to surface fatigue.

4.3. Rear Cross-Section Crack

Another potential fatigue failure of the FS may originate at the rear cross-section, as noted in [72]. The stress concentration in this area is exacerbated by the coning angle, a deformation phenomenon unique to harmonic drives. Due to the specific manner in which the FS deforms, the WG-FS interface does not uniformly span the entire thickness of the elliptical bearing. Instead, only a portion of the WG outer ring makes full contact with the inner surface of the FS cup, particularly near the rear cross-section. This uneven contact distribution results in localized stress peaks that can become sites for crack nucleation.

However, since the rear cross-section is not as critical to the harmonic drive's core operational function, detecting a crack in this region during its early stages may be particularly challenging. The influence of such a crack on the robot's performance would likely be minimal at first, with any abnormalities in joint signals being masked by the overall system noise. This makes early fault detection in this area more complex, requiring advanced signal processing techniques to differentiate subtle indicators of failure from background noise.

Despite its seemingly lower significance, a crack in the rear cross-section can still progress to a complete breakage if left unchecked, as demonstrated in [85]. In their study, a harmonic drive experienced catastrophic failure initiated by a manufacturing defect

in the rear cross-section. The failure evolved through fatigue fracture, which eventually compromised the entire system. This case underlines the importance of manufacturing precision and thorough quality control in ensuring the long-term reliability of harmonic drives, especially in mission-critical applications where unexpected failures can lead to significant downtime or even equipment damage.

In summary, while the rear cross-section may not play a primary role in the harmonic drive's gear engagement, it can still become a critical failure point under certain conditions. Detecting and mitigating such fatigue-induced failures requires a robust monitoring strategy that accounts for stress distribution, manufacturing variances, and real-time system noise.

The rear cross-section of the flexspline can experience both mechanical and thermal stresses during operation. A thermo-mechanical model that incorporates temperature variations and mechanical loads can predict the formation of cracks due to combined effects.

4.4. Diaphragm Crack

A crack at the diaphragm–boss interface is another common failure mode in harmonic drives, as identified in [86]. This failure pattern is attributed to a combination of factors, including the deflection of the FS induced by the WG and external load conditions. The output torque applied to the system intensifies the shear stress on the FS diaphragm, accelerating crack initiation and propagation in this critical region.

The diaphragm–boss interface plays a crucial role in harmonic drives, as it serves as the connection point between the oscillatory deformation of the FS and the rotational motion of the gearbox output shaft. A crack at this junction could significantly impact the overall system performance by reducing the torsional stiffness of the FS. Torsional stiffness is essential for maintaining the precision of motion transmission within the harmonic drive, and any reduction in this parameter can lead to a notable increase in joint position error.

Such an error, which manifests as a discrepancy between the commanded and actual joint positions, can affect the accuracy and repeatability of industrial robots, particularly in applications requiring high precision, such as pick-and-place tasks, welding, or machining. The degradation in torsional stiffness can also amplify the effects of backlash and vibration, further compromising the robot's performance.

Fatigue failure at the diaphragm–boss interface tends to be progressive, meaning that the crack may grow slowly at first but can lead to catastrophic failure if not detected early. Given its location, the crack might not immediately produce significant noise or vibration detectable by standard diagnostic methods. Therefore, condition monitoring techniques, such as vibration analysis or torque ripple detection, can play a pivotal role in identifying early signs of diaphragm cracking. Advanced diagnostic tools could potentially detect slight changes in the system's dynamic behavior before the crack leads to a complete loss of functionality.

Because the diaphragm of the flexspline is a thin-walled structure, a thin shell finite element model can simulate crack initiation and propagation in the diaphragm by analyzing the stress concentrations and material behavior under load.

Diaphragm cracks can result from local buckling of the thin structure due to compressive forces. A buckling analysis combined with fracture mechanics can predict when and where cracks will form due to buckling-induced stress concentrations.

Diaphragms undergo repeated flexing during operation, which can lead to fatigue cracks. A cyclic fatigue model (e.g., Paris' Law or S-N curves) can estimate crack initiation and growth based on the number of cycles and stress levels.

In conclusion, a crack at the diaphragm–boss interface is a critical failure mode in harmonic drives that can significantly impact system accuracy and reliability. Addressing this failure pattern requires comprehensive fatigue analysis, real-time monitoring of dynamic parameters, and robust predictive maintenance strategies to prevent unexpected breakdowns in industrial applications.

5. Fault-to-Failure Mechanisms and Failure Mode, Effects, and Criticality Analysis of a Harmonic Drive

As inferred from the previous discussion, the fault-to-failure mechanism in harmonic drives is a multifaceted process, beginning with root causes such as cyclic loading, thermal stress, improper lubrication, and material fatigue. These root causes set off a cascade of stressors that initiate early faults within the drive's components. For example, cyclic loading induces recurring mechanical strain on the flexspline, creating wear patterns and micro-cracks that can worsen over time (Table 1).

From these initial conditions, faults such as wear, pitting, and cracking begin to manifest, each with unique characteristics and impacts on the harmonic drive's functionality. Wear is generally linked to high friction and repetitive motion, gradually degrading the drive's contact surfaces. Pitting, a form of surface fatigue, occurs under high-load conditions and is particularly damaging to the teeth of the flexspline, leading to rough surfaces that can propagate further faults. Cracks, often originating from both mechanical loading and thermal stress, may initially appear as microscopic fissures but can quickly expand due to the continuous stresses imposed during drive operation.

Fault progression toward complete failure is strongly influenced by several parameters: load intensity, operating temperature, vibration frequency, lubrication quality, and the friction coefficient. For instance, as load intensity increases, wear and pitting accelerate, while high temperatures exacerbate material degradation and crack propagation. Vibration frequency affects the rate at which cyclic loading impacts the drive, hastening fatigue-related failures. Additionally, poor lubrication quality increases frictional forces, leading to rapid wear and heat buildup, which can catalyze multiple fault types simultaneously. Recognizing these parameters and their roles in fault progression is vital for effective monitoring and predictive maintenance, as it enables early interventions to manage initial faults before they advance to critical stages, thus enhancing the reliability and lifespan of harmonic drives in demanding industrial applications.

Table 1. Fault-to-failure paths in harmonic drives: root causes, fault initiation, progression, and failure modes.

Fault Type	Root Causes	Fault Initiation	Progression	Failure Mode
Wear	High friction, cyclic loading, insufficient lubrication	Surface erosion on flexspline and components	Increased backlash, reduced precision, degraded component strength	Misalignment, loss of torque efficiency, drive failure
Pitting	High cyclic stress, heavy loads, material fatigue	Formation of pits or craters on flexspline teeth	Surface roughness, disrupted motion	Tooth deformation, material fragmentation, impaired torque transmission
Cracking	Cyclic loading, thermal stress, material fatigue	Micro-cracks at high-stress points on flexspline	Crack propagation under loading cycles	Loss of structural integrity, component detachment, drive failure
Ratcheting/Buckling	Excessive axial or compressive load	Deformation of flexspline under load	Reduced engagement and alignment	Misalignment, improper interface, drive function loss

To identify the most effective failure modes related to harmonic drives and their impact on robot performance, conducting an FMECA (Failure Modes, Effects, and Criticality Analysis) is essential. The results of this analysis provide valuable insight into which faults and failures should be simulated using the high-fidelity (HF) model of the harmonic drive. Although the presented work focuses on a UR5 cobot use case, the methodology has general applicability. However, since robot components are not standardized across

different manufacturers, FMECAs for manipulators from various brands or models may yield slightly different results compared to those shown in Table 2.

Due to the lack of available field data, often restricted to harmonic drive and robot manufacturers, the proposed analysis should be seen as a preliminary insight into harmonic drive failure modes. Nevertheless, the values for severity (S), occurrence (O), and detectability (D) reported in Table 1 are consistent with the data from the literature and align with the criteria outlined in the 2020 SAE International report. These indices were defined using a 1-to-10 scale:

- Severity (S): Measures the impact of the failure on the entire system. A score of 1 indicates no impact, while a score of 10 signifies a total system breakdown with possible operator injuries and no prior warning.
- Occurrence (O): Represents the likelihood of a failure mode occurring over a specific period. A score of 1 corresponds to an extremely unlikely event, while a score of 10 indicates inevitability.
- Detectability (D): Reflects the probability of detecting symptoms or indicators of a particular failure mode through sensors or manual inspection. A higher score indicates a lower likelihood of detection. The detectability values are assigned based on the likelihood of identifying the failure mode without dismantling the gearbox from the robot. This is typically evaluated through the analysis of vibration signals or data directly from the manipulator.

To determine the Risk Priority Number (RPN), the three scores are multiplied together. A higher RPN indicates a more critical failure mode. However, it is essential to interpret the final scores with caution due to certain limitations of this method. In the case study presented, wear at the WG-FS interface emerges as one of the most significant failure modes in harmonic drives. This is primarily due to the inevitability of wear in these drives, which is often difficult to detect through robot signal analysis. Consequently, the combination of high occurrence and low detectability scores results in a heightened RPN. A similar situation is observed with lubricant degradation; assessing the grease condition within a sealed robot joint necessitates disassembly. While dynamic parameter identification algorithms might provide estimates of the grease's health, the reliability of this method can be compromised by other influences, such as wear in the teeth or bearings, which may affect friction coefficients.

In situations like these, the Severity Index becomes pivotal in risk assessment. When failures have similar RPNs, priority is given to those with higher severity ratings. For instance, a crack at the FS tooth root surface is of far greater concern than one at the tooth tip, even if their RPNs are similar. Additionally, since harmonic drives used in the UR5 robot have high backup ratios, a crack would be unlikely to propagate through the rim, which mitigates the risk of catastrophic rim fracture. Consequently, despite the potential severity of a rim fracture, it may not be a priority in this case study due to the low probability of occurrence.

Particularly noteworthy is the bottom section of the FMECA table, which lists failure modes like buckling and ratcheting. Despite their high severity ratings, these failure modes have relatively low RPNs. This is because they can be easily avoided through proper implementation and operational practices. Furthermore, they can be detected early by the robot itself or through the heightened vibrations they induce in the robot arm. Proper collision avoidance algorithms and routine maintenance can significantly reduce the likelihood of such failures, ensuring the safe and reliable operation of the manipulator.

In FMECA, failures with the highest RPNs and severity values are prioritized, as they pose the greatest threats to the harmonic drive's performance and reliability. For instance, WG-FS interface wear, with an RPN of 180, is highly critical due to its frequent occurrence and substantial impact on efficiency, lubricant contamination, and alignment. Additionally, rear cross-section cracks display a high severity (S = 9) and an RPN of 162, highlighting their potential to cause total gearbox breakage and severe vibration, jeopardizing the drive's structural integrity.

Table 2. Detailed failure mode, effects, and criticality analysis (FMECA) of a harmonic drive used in the UR5 cobot [8].

Failure Mode	Effect	S	O	D	RPN
WG-FS interface wear	Lubricant contamination, efficiency loss, increment in the WG-FS sliding movement	3	10	6	180
Rear cross-section crack	Vibration, total breakage of the gearbox	9	2	9	162
Lubricant degradation	Wear, increment of the wave generator axial load	2	10	8	160
Tooth wear	Backlash, vibration, uneven load distribution, lubricant contamination	3	10	4	120
Root tooth crack	Excessive vibration, efficiency degradation	7	4	4	112
Diaphragm crack	Vibration, decrement of the torsional stiffness, efficiency degradation	4	3	9	108
Tip tooth crack	Vibration, efficiency degradation	2	5	9	90
Pitting	Lubricant contamination and degradation, wear	1	10	9	90
Wave generator wear	Vibration, lubricant contamination, efficiency degradation	2	7	6	84
Rim crack	Excessive vibration, uneven load distribution, efficiency and accuracy degradation, total breakage of the flexspline	9	1	4	36
Buckling	Loss of FS flexibility, excessive vibration and wear	9	1	1	9
Ratcheting	Flexspline—circular spline eccentricity, vibration, and wear	7	1	1	7

However, it is essential to recognize that the priority of these faults can vary depending on the application. For example, in collaborative robots (cobots) operating near humans, rim cracks (S = 9) may be particularly critical due to the potential for misalignment and abrupt motion changes that could pose safety risks. In contrast, for aerospace applications, buckling (S = 9) becomes more significant as it compromises the precision and durability required in high-stake environments. Therefore, identifying the most critical faults requires an understanding of the specific operational demands, as these factors influence which failure modes should be prioritized for maintenance and monitoring in each application.

In summary, while FMECA provides a structured approach to identifying and prioritizing failure modes in harmonic drives, its effectiveness depends on the quality and availability of data. For failure modes with high severity scores, special attention should be given to both early detection strategies and preventive measures, which can significantly extend the operational life of the system and reduce the risk of catastrophic failures.

6. Conclusions

This study provides a comprehensive analysis of the fault-to-failure mechanisms in harmonic drives, specifically detailing how root causes like cyclic loading, thermal stress, and inadequate lubrication initiate and propagate faults over time. Through a systematic exploration of failure types—including wear, pitting, cracking, buckling, and thermal deformation—this work illustrates how each fault progresses from initial degradation to complete failure, emphasizing key parameters that influence these pathways. The presented fault-to-failure descriptions offer valuable insights for understanding how minor degradations can escalate under specific operational conditions, enabling proactive strategies for predictive maintenance.

The FMECA results further prioritize failure modes by assessing their Risk Priority Numbers (RPNs) and severity values, identifying WG-FS interface wear and rear cross-section cracks as particularly high-risk due to their likelihood and impact on drive reliability. However, our analysis also highlights that fault prioritization must account for the appli-

cation context. For example, rim cracks are critical in collaborative robotic applications due to potential safety risks, while buckling holds greater priority in aerospace settings where precision and durability are paramount. These findings underscore the importance of tailored maintenance approaches that consider both the fault-to-failure mechanisms and the specific requirements of each application. This study thus provides a valuable framework for guiding PHM and predictive maintenance strategies, helping to enhance the reliability and lifespan of harmonic drives in diverse industrial environments.

This study offers valuable insights into harmonic drive failure mechanisms behind harmonic drive failures and offers practical recommendations for developing robust maintenance strategies. By focusing on early fault detection, predictive maintenance, and improving the fault tolerance of key robotic components, this study contributes to the ongoing effort to enhance the reliability of industrial automation, ensuring safer and more efficient operations in high-stake environments.

Author Contributions: Conceptualization, R.G., A.C.B. and A.D.M.; data curation, A.C.B.; formal analysis, R.G.; funding acquisition, M.S.; investigation, R.G.; methodology, R.G.; project administration, M.S.; resources, M.S.; supervision, M.S.; validation, A.C.B.; visualization, A.C.B.; writing—original draft preparation, R.G.; writing—review and editing, A.C.B. and A.D.M. All authors have read and agreed to the published version of the manuscript.

Funding: This research received no external funding.

Data Availability Statement: The original contributions presented in this study are included in the article. Further inquiries can be directed to the corresponding author.

Conflicts of Interest: The authors declare no conflicts of interest.

Abbreviations

The following abbreviations are used in this manuscript:

FMECA	Failure Mode, Effects, and Criticality Analysis
CBM	Condition-Based Maintenance
PHM	Prognostics and Health Management
RUL	Remaining Useful Life
DDM	Data-driven model
FTA	Fault Tree Analysis
TLE	Top-level event
HR	Harmonic drive
WG	Wave generator
FS	Flexspline
CS	Circular spline
CZM	Cohesive zone model

References

1. Tuttle, T.D. Understanding and Modeling the Behavior of a Harmonic Drive Gear Transmission. Ph.D. Thesis, Massachusetts Institute of Technology, Cambridge, MA, USA, 1992.
2. Kennedy, C.W.; Desai, J.P. Modeling and control of the Mitsubishi PA-10 robot arm harmonic drive system. *IEEE/ASME Trans. Mechatronics* **2005**, *10*, 263–274. [CrossRef]
3. Ueura, K.; Slatter, R. Development of the harmonic drive gear for space applications. In Proceedings of the 8th European Space Mechanisms and Tribology Symposium, Toulouse, France, 29 September–1 October 1999; Volume 438, p. 259.
4. Taghirad, H.; Be´ langer, P. Modeling and parameter identification of harmonic drive systems. *J. Dyn. Sys. Meas. Control.* **1998**, *120*, 439–444. [CrossRef]
5. Routh, B. Design aspects of harmonic drive gear and performance improvement of its by problems identification: A review. In Proceedings of the AIP Conference Proceedings, Karnataka, India, 29–31 January 2018; AIP Publishing: College Park, MD, USA, 2018; Volume 1943.
6. Wu, G.; Peng, X. Load Distribution among the Teeth of Flexspline of Harmonic Drive with Double Circular-arc Tooth Profile. In Proceedings of the 4th International Conference on Computer, Mechatronics, Control and Electronic Engineering, Hangzhou, China, 28–29 September 2015; Atlantis Press: Amsterdam, The Netherlands, 2015; pp. 1083–1086.

7. Chen, G.; Li, H.; Liu, Y. Double-arc harmonic gear profile design and meshing analysis for multi-section conjugation. *Adv. Mech. Eng.* **2019**, *11*, 1687814019850656. [CrossRef]
8. Raviola, A.; De Martin, A.; Guida, R.; Jacazio, G.; Mauro, S.; Sorli, M. Harmonic drive gear failures in industrial robots applications: An overview. In Proceedings of the PHM Society European Conference, Virtual, 29 November–2 December 2021; Volume 6, p. 11.
9. Sensinger, J.W.; Lipsey, J.H. Cycloid vs. harmonic drives for use in high ratio, single stage robotic transmissions. In Proceedings of the 2012 IEEE International Conference on Robotics and Automation, Saint Paul, MN, USA, 14–18 May 2012; IEEE: Piscataway, NJ, USA, 2012; pp. 4130–4135.
10. Junyang, L.; Jiaxun, W.; Kaijie, F.; Zhonglai, W. Accelerated life model for harmonic drive under adhesive wear. *Tribology* **2016**, *36*, 297–303.
11. Yu, Z.; Ling, S.; Wang, X.; Zheng, Y. Modeling harmonic drive with small deformation of flexspline and assessment of tooth wear by sliding coefficient. *Proc. Inst. Mech. Eng. Part J J. Eng. Tribol.* **2023**, *237*, 431–450. [CrossRef]
12. Schäfer, I.; Bourlier, P.; Hantschack, F.; Roberts, E.; Lewis, S.; Forster, D.; John, C. Space lubrication and performance of harmonic drive gears. In Proceedings of the 11th European Space Mechanisms and Tribology Symposium, ESMATS 2005, Lucerne, Switzerland, 21–23 September 2005; Volume 591, pp. 65–72.
13. Li, Y.; Zhang, G.; Zhang, Y. Thermal–mechanical coupling deformation difference analysis for the flexspline of a harmonic drive. *Rev. Adv. Mater. Sci.* **2022**, *61*, 698–710. [CrossRef]
14. Lu, B.; Durocher, D.B.; Stemper, P. Predictive maintenance techniques. *IEEE Ind. Appl. Mag.* **2009**, *15*, 52–60. [CrossRef]
15. Prajapati, A.; Bechtel, J.; Ganesan, S. Condition based maintenance: A survey. *J. Qual. Maint. Eng.* **2012**, *18*, 384–400. [CrossRef]
16. Yucesan, Y.A.; Dourado, A.; Viana, F.A. A survey of modeling for prognosis and health management of industrial equipment. *Adv. Eng. Inform.* **2021**, *50*, 101404. [CrossRef]
17. Ayankoso, S.; Kaigom, E.; Louadah, H.; Faham, H.; Gu, F.; Ball, A. A Hybrid Digital Twin Scheme for the Condition Monitoring of Industrial Collaborative Robots. *Procedia Comput. Sci.* **2024**, *232*, 1099–1108. [CrossRef]
18. Grosso, L.A.; De Martin, A.; Jacazio, G.; Sorli, M. Development of data-driven PHM solutions for robot hemming in automotive production lines. *Int. J. Progn. Health Manag.* **2020**, *11*. [CrossRef]
19. De Martin, A.; Jacazio, G.; Vachtsevanos, G. Windings fault detection and prognosis in electro-mechanical flight control actuators operating in active-active configuration. *Int. J. Progn. Health Manag.* **2017**, *8*. [CrossRef]
20. Autin, S.; Socheleau, J.; Dellacasa, A.; De Martin, A.; Jacazio, G.; Vachtsevanos, G. Feasibility Study of a PHM System for Electro-hydraulic Servo-actuators for Primary Flight Controls. In Proceedings of the Annual Conference of the PHM Society, Philadelphia, PA, USA, 24–27 September 2018; Volume 10.
21. Nesci, A.; De Martin, A.; Jacazio, G.; Sorli, M. Detection and prognosis of propagating faults in flight control actuators for helicopters. *Aerospace* **2020**, *7*, 20. [CrossRef]
22. Wang, C.; Yang, J.; Jie, H.; Zhao, Z.; Wang, W. An energy-efficient mechanical fault diagnosis method based on neural dynamics-inspired metric SpikingFormer for insufficient samples in industrial Internet of Things. *IEEE Internet Things J.* **2024**, *early access*. [CrossRef]
23. Wang, C.; Yang, J.; Jie, H.; Tao, Z.; Zhao, Z. A lightweight progressive joint transfer ensemble network inspired by the Markov process for imbalanced mechanical fault diagnosis. *Mech. Syst. Signal Process.* **2025**, *224*, 111994. [CrossRef]
24. Wang, C.; Tian, B.; Yang, J.; Jie, H.; Chang, Y.; Zhao, Z. Neural-transformer: A brain-inspired lightweight mechanical fault diagnosis method under noise. *Reliab. Eng. Syst. Saf.* **2024**, *251*, 110409. [CrossRef]
25. Wang, C.; Yang, J.; Jie, H.; Tian, B.; Zhao, Z.; Chang, Y. An uncertainty perception metric network for machinery fault diagnosis under limited noisy source domain and scarce noisy unknown domain. *Adv. Eng. Inform.* **2024**, *62*, 102682. [CrossRef]
26. Wallén, J. *The History of the Industrial Robot*; Linköping University Electronic Press: Linkoping, Sweden, 2008.
27. Grau, A.; Indri, M.; Bello, L.L.; Sauter, T. Robots in industry: The past, present, and future of a growing collaboration with humans. *IEEE Ind. Electron. Mag.* **2020**, *15*, 50–61. [CrossRef]
28. Hornung, R.; Urbanek, H.; Klodmann, J.; Osendorfer, C.; Van Der Smagt, P. Model-free robot anomaly detection. In Proceedings of the 2014 IEEE/RSJ International Conference on Intelligent Robots and Systems, Chicago, IL, USA, 14–18 September 2014; IEEE: Piscataway, NJ, USA, 2014; pp. 3676–3683.
29. Mauro, S.; Scimmi, L.S.; Pastorelli, S. Collision avoidance system for collaborative robotics. In Proceedings of the Advances in Service and Industrial Robotics: Proceedings of the 26th International Conference on Robotics in Alpe-Adria-Danube Region, RAAD 2017, Turin, Italy, 21–23 June 2017; Springer: Berlin/Heidelberg, Germany, 2018; pp. 344–352.
30. Polenghi, A.; Cattaneo, L.; Macchi, M. A framework for fault detection and diagnostics of articulated collaborative robots based on hybrid series modelling of Artificial Intelligence algorithms. *J. Intell. Manuf.* **2024**, *35*, 1929–1947. [CrossRef]
31. Abd Majid, M.A.; Fudzin, F. Study on robots failures in automotive painting line. *Asian Res. Publ. Netw.* **2017**, *12*, 62–67.
32. Qiao, G.; Weiss, B.A. Accuracy degradation analysis for industrial robot systems. In Proceedings of the International Manufacturing Science and Engineering Conference, Los Angeles, CA, USA, 4–8 June2017; American Society of Mechanical Engineers: New York, NY, USA, 2017; Volume 50749, p. V003T04A006.
33. Zhou, Q.; Wang, Y.; Xu, J. A summary of health prognostics methods for industrial robots. In Proceedings of the 2019 Prognostics and System Health Management Conference (PHM-Qingdao), Qingdao, China, 25–27 October 2019; IEEE: Piscataway, NJ, USA, 2019; pp. 1–6.

34. Almurib, H.A.; Al-Qrimli, H.F.; Kumar, N. A review of application industrial robotic design. In Proceedings of the 2011 Ninth International Conference on ICT and Knowledge Engineering, Bangkok, Thailand, 12–13 January 2012; IEEE: Piscataway, NJ, USA, 2012; pp. 105–112.
35. Walker, I.D.; Cavallaro, J.R. Failure mode analysis for a hazardous waste clean-up manipulator. *Reliab. Eng. Syst. Saf.* **1996**, *53*, 277–290. [CrossRef]
36. Ferguson, T.A.; Lu, L. Fault tree analysis for an inspection robot in a nuclear power plant. In Proceedings of the IOP Conference Series: Materials Science and Engineering, Busan, Republic of Korea, 25–27 August 2017; IOP Publishing: Bristol, UK, 2017; Volume 235, p. 012003.
37. Lee, W.S.; Grosh, D.L.; Tillman, F.A.; Lie, C.H. Fault tree analysis, methods, and applications: A review. *IEEE Trans. Reliab.* **1985**, *34*, 194–203. [CrossRef]
38. Ruijters, E.; Stoelinga, M. Fault tree analysis: A survey of the state-of-the-art in modeling, analysis and tools. *Comput. Sci. Rev.* **2015**, *15*, 29–62. [CrossRef]
39. Rider, R.; Harvey, S.; Chandler, H. Fatigue and ratcheting interactions. *Int. J. Fatigue* **1995**, *17*, 507–511. [CrossRef]
40. Hu, Y.; Wang, Y.; Hu, K.; Li, W. Adaptive obstacle avoidance in path planning of collaborative robots for dynamic manufacturing. *J. Intell. Manuf.* **2023**, *34*, 789–807. [CrossRef]
41. Zhang, Q.; Huang, D.; Gu, J. Buckling Analysis for Flexspline Structure in Harmonic Drive with FEM. *J. Mech. Transm.* **2017**, *41*, 128–130.
42. Schäfer, I. *Improving the Reliability of EMA by Using Harmonic Drive Gears*; Technical Report, SAE Technical Paper; SAE: Atlanta, GA, USA, 2005. [CrossRef]
43. Haddadin, S.; De Luca, A.; Albu-Schäffer, A. Robot collisions: A survey on detection, isolation, and identification. *IEEE Trans. Robot.* **2017**, *33*, 1292–1312. [CrossRef]
44. Ambroziak, A.; Kłosowski, P. The elasto-viscoplastic Chaboche model. *TASK Q. Sci. Bull. Acad. Comput. Cent. Gdan.* **2006**, *10*, 49–61.
45. Budaházy, V.; Dunai, L. Parameter-refreshed Chaboche model for mild steel cyclic plasticity behaviour. *Period. Polytech. Civ. Eng.* **2013**, *57*, 139–155. [CrossRef]
46. Halama, R.; Sedlák, J.; Šofer, M. Phenomenological modelling of cyclic plasticity. *Numer. Model.* **2012**, *1*, 329–354.
47. Rychlewski, J. On Hooke's law. *J. Appl. Math. Mech.* **1984**, *48*, 303–314. [CrossRef]
48. Bouaziz, O.; Kim, H.S.; Lee, J.; Estrin, Y. Bauschinger effect or kinematic hardening: Bridging microstructure and continuum mechanics. *Met. Mater. Int.* **2023**, *29*, 280–292. [CrossRef]
49. Li, J.Y.; Wang, J.X.; Zhou, G.W.; Pu, W.; Wang, Z.H. Accelerated life testing of harmonic driver in space lubrication. *Proc. Inst. Mech. Eng. Part J J. Eng. Tribol.* **2015**, *229*, 1491–1502. [CrossRef]
50. Roberts, E.W.; Bridgeman, P.; Jansson, M.; Schulke, M.; Tvaruzka, A. The performance and life of fluid-lubricated Harmonic Drive® Gears. In Proceedings of the 16th European Space Mechanisms and Tribology Symposium 2015, Bilbao, Spain, 23–25 September 2015; pp. 23–25.
51. Kovincic, N.; Müller, A.; Gattringer, H.; Weyrer, M.; Schlotzhauer, A.; Brandstötter, M. Dynamic parameter identification of the Universal Robots UR5. In Proceedings of the Austrian Robotics Workshop, Steyr, AT, USA, 9–10 May 2019.
52. Ueura, K.; Kiyosawa, Y.; Kurogi, J.; Kanai, S.; Miyaba, H.; Maniwa, K.; Suzuki, M.; Obara, S. Tribological aspects of a strain wave gearing system with specific reference to its space application. *Proc. Inst. Mech. Eng. Part J J. Eng. Tribol.* **2008**, *222*, 1051–1061. [CrossRef]
53. Routh, B.; Maiti, R.; Ray, A.K. Analysis of coning and lubrication at flexspline cup and cam interface in conventional harmonic drives. *Ind. Lubr. Tribol.* **2017**, *69*, 817–827. [CrossRef]
54. Goncalves, D.; Graca, B.; Campos, A.V.; Seabra, J. Film thickness and friction behaviour of thermally aged lubricating greases. *Tribol. Int.* **2016**, *100*, 231–241. [CrossRef]
55. Laidler, K.J. The development of the Arrhenius equation. *J. Chem. Educ.* **1984**, *61*, 494. [CrossRef]
56. Peleg, M.; Normand, M.D.; Corradini, M.G. The Arrhenius equation revisited. *Crit. Rev. Food Sci. Nutr.* **2012**, *52*, 830–851. [CrossRef]
57. Masoumi, M.; Alimohammadi, H. An investigation into the vibration of harmonic drive systems. *Front. Mech. Eng.* **2013**, *8*, 409–419. [CrossRef]
58. Guida, R.; Bertolino, A.C.; De Martin, A.; Mauro, S.; Sorli, M. Effect of Wave Generator Misalignment on the Strain Wave Gear Hysteretic Behavior in a Rotary Electro-Mechanical Actuator. In Proceedings of the IFToMM World Congress on Mechanism and Machine Science, Tokyo, Japan, 5–10 November 2023; Springer: Berlin/Heidelberg, Germany, 2023; pp. 154–162.
59. Glodež, S.; Ren, Z.; Flašker, J. Simulation of surface pitting due to contact loading. *Int. J. Numer. Methods Eng.* **1998**, *43*, 33–50. [CrossRef]
60. Kamal, M.; Rahman, M. Advances in fatigue life modeling: A review. *Renew. Sustain. Energy Rev.* **2018**, *82*, 940–949. [CrossRef]
61. Larrosa, N.; Akid, R.; Ainsworth, R. Corrosion-fatigue: A review of damage tolerance models. *Int. Mater. Rev.* **2018**, *63*, 283–308. [CrossRef]
62. Jaber, A.A.; Bicker, R. Fault diagnosis of industrial robot gears based on discrete wavelet transform and artificial neural network. *Insight-Non Test. Cond. Monit.* **2016**, *58*, 179–186. [CrossRef]

63. Zhang, X.; Kang, J.; Hao, L.; Cai, L.; Zhao, J. Bearing fault diagnosis and degradation analysis based on improved empirical mode decomposition and maximum correlated kurtosis deconvolution. *J. Vibroengineering* **2015**, *17*, 243–260.
64. Wen, J.; Gao, H.; Zhang, J. Bearing remaining useful life prediction based on a nonlinear wiener process model. *Shock Vib.* **2018**, *2018*, 4068431. [CrossRef]
65. Wang, Y.; Chang, M.; Huang, X.; Li, Y.; Tang, J. Cutting tool wear prediction based on the multi-stage Wiener process. *Int. J. Adv. Manuf. Technol.* **2023**, *129*, 5319–5333. [CrossRef]
66. Sahoo, V.; Maiti, R. State of stress in strain wave gear flexspline cup on insertion of drive cam-experiment and analysis. In Proceedings of the World Congress on Engineering, London, UK, 29 June–1 July 2016; Volume 2.
67. Mahanto, B.S.; Sahoo, V.; Maiti, R. Effect of cam insertion on stresses in harmonic drive in industrial robotic joints. *Procedia Comput. Sci.* **2018**, *133*, 432–439. [CrossRef]
68. Kauzlarich, J. The Palmgren-Miner rule derived. In *Tribology Series*; Elsevier: Amsterdam, The Netherlands, 1989; Volume 14, pp. 175–179.
69. Morales-Espejel, G.; Rycerz, P.; Kadiric, A. Prediction of micropitting damage in gear teeth contacts considering the concurrent effects of surface fatigue and mild wear. *Wear* **2018**, *398*, 99–115. [CrossRef]
70. Archard, J.F. Contact and rubbing of flat surfaces. *J. Appl. Phys.* **1953**, *24*, 981–988. [CrossRef]
71. Archard, J.; Hirst, W. The Wear of Materials under unlubricated Conditions. *Proc. R. Soc. Lond. A* **1958**, *236*, 71–73.
72. Dong, H.; Zhu, Z.; Zhou, W.; Chen, Z. Dynamic Simulation of Harmonic Gear Drives Considering Tooth Profiles Parameters Optimization. *J. Comput.* **2012**, *7*, 1429–1436. [CrossRef]
73. Wang, W. Early detection of gear tooth cracking using the resonance demodulation technique. *Mech. Syst. Signal Process.* **2001**, *15*, 887–903. [CrossRef]
74. Park, K.; Paulino, G.H. Cohesive zone models: A critical review of traction-separation relationships across fracture surfaces. *Appl. Mech. Rev.* **2011**, *64*, 060802. [CrossRef]
75. Paris, P.; Erdogan, F. A critical analysis of crack propagation laws. *J. Basic Eng.* **1963**, *85*, 528–533. [CrossRef]
76. Zheng, J.; Yang, W. Failure analysis of a flexspline of harmonic gear drive in STC industrial robot: Microstructure and stress distribution. In Proceedings of the IOP Conference Series: Materials Science and Engineering, Harbin, China, 4–6 May 2018; IOP Publishing: Bristol, UK, 2018; Volume 452, p. 042148.
77. Lewicki, D.G.; Ballarini, R. Effect of rim thickness on gear crack propagation path. *J. Mech. Des.* **1997**, *119*, 88–95. [CrossRef]
78. Curà, F.; Mura, A.; Rosso, C. Investigation about crack propagation paths in thin rim gears. *Frat. Ed Integrità Strutt.* **2014**, *8*, 446–453. [CrossRef]
79. Lewicki, D.G. Gear Crack Propagation Path Studies-Guidelines for Ultra-Safe Design. *J. Am. Helicopter Soc.* **2002**, *47*, 64–72. [CrossRef]
80. Routh, B.; Maiti, R. On a gearing problem in conventional harmonic drives with involute toothed gear set. In Proceedings of the International Design Engineering Technical Conferences and Computers and Information in Engineering Conference, Washington, DC, USA, 28–31 August 2011; Volume 54853, pp. 481–489.
81. Kayabasi, O.; Erzincanli, F. Shape optimization of tooth profile of a flexspline for a harmonic drive by finite element modelling. *Mater. Des.* **2007**, *28*, 441–447. [CrossRef]
82. Ma, H.; Pang, X.; Zeng, J.; Wang, Q.; Wen, B. Effects of gear crack propagation paths on vibration responses of the perforated gear system. *Mech. Syst. Signal Process.* **2015**, *62*, 113–128. [CrossRef]
83. Meng, Z.; Shi, G.; Wang, F. Vibration response and fault characteristics analysis of gear based on time-varying mesh stiffness. *Mech. Mach. Theory* **2020**, *148*, 103786. [CrossRef]
84. Frank, F.C.; Lawn, B. On the theory of Hertzian fracture. *Proc. R. Soc. London. Ser. A Math. Phys. Sci.* **1967**, *299*, 291–306.
85. Smith, J.D.; Nick, A.J.; Schuler, J.M.; Kennett, A.; Dillon, R.P. Cryobotics: Extreme cold environment testing of strain wave gear sets. In Proceedings of the 2019 IEEE Aerospace Conference, Big Sky, MT, USA, 2–9 March 2019; IEEE: Piscataway, NJ, USA, 2019; pp. 1–10.
86. Li, S. Diaphragm stress analysis and fatigue strength evaluation of the flex-spline, a very thin-walled spur gear used in the strain wave gearing. *Mech. Mach. Theory* **2016**, *104*, 1–16. [CrossRef]